Designing Plasmon-Enhanced Thermochromic Films Using a Vanadium Dioxide Nanoparticle Elastomeric Composite

Taylor Moot, Cass Palin, Sorin Mitran, James F. Cahoon, and Rene Lopez*

Vanadium dioxide (VO$_2$) is a common material for use in thermochromic windows due to a semiconductor-to-metal transition (SMT) that is coupled with a change in infrared opacity. Commercialization of VO$_2$-based thermochromic technology is hampered by relatively expensive synthesis and film fabrication techniques as well as overall low performance as a window material. Here, simulations that indicate the plasmon resonance of VO$_2$ nanoparticles in a composite film, which can be tuned to achieve record performance values, are reported. These simulations are experimentally verified by fabricating a VO$_2$ nanoparticle composite in an elastomeric matrix using low-temperature and atmospheric processing conditions. The optical properties of the films are analyzed, yielding visible transmittance and infrared modulation values within the range of top-performing thermochromic windows. In addition, an improvement in performance is observed upon stretching the films, an effect that can be attributed to a local refractive index modulation. The results highlight the potential use of elastomeric composites as a low-cost route to higher-performance smart windows.

1. Introduction

Approximately 40% of worldwide energy consumption is used to heat and cool interior climates.[1] Much of this energy usage is wasted through windows, placing an unnecessary strain on an energy supply that will need to be increased 56% by 2040.[2] In order to mitigate losses through windows, an efficient thermochromic "smart" window that passively reduces heat exchange by altering its infrared (IR) opacity based on temperature is needed. To date, the most promising material for this application is vanadium dioxide (VO$_2$), a well-known thermochromic material whose key properties were discovered

T. Moot, C. Palin, Prof. J. F. Cahoon
Department of Chemistry
University of North Carolina at Chapel Hill
NC 27599-3290, USA
S. Mitran
Department of Mathematics
University of North Carolina at Chapel Hill
NC 27599-3250, USA
Prof. R. Lopez
Department of Physics and Astronomy
University of North Carolina at Chapel Hill
NC 27599, USA
E-mail: rln@email.unc.edu

in 1959.[3] VO$_2$ passively switches from an IR-transparent semiconductor monoclinic (M) phase to an IR-opaque metal rutile (R) phase when heated above 68 °C.[4,5] This semiconductor-to-metal transition (SMT), with its coupled change in optical properties, allows VO$_2$ to facilitate heating at low temperatures with VO$_2$ (M) and minimize radiative heating at high temperatures with VO$_2$ (R). Until recently, most studies on the thermochromic properties of this material have been focused on pure VO$_2$ thin films, which have reached top performance values of 47.2% visible transmittance and 15.1% IR modulation with the use of an antireflective overcoating.[6–10] The main drawback of thin films is that in order to reach a reasonable IR modulation a sufficiently thick film must be used, and the necessary thickness results in low visible transmittance. Additionally, VO$_2$ thin-film fabrication usually requires high annealing temperatures and does not lend itself well to manufacturing on the industrial scale or to retrofitting of existing windows.

The ideal thermochromic coating would be capable of high visible transmittance as well as high IR modulation and would be processed on a flexible substrate using a facile, low-temperature synthesis, and fabrication method. A viable path toward this goal is VO$_2$ nanoparticles suspended in polymer thin films.[11] In fact, the use of various VO$_2$ nanoparticle composites has given impressive results, with many designs already outperforming the traditional thin films.[12–16] For instance, a VO$_2$ nanoparticle hydrogel composite currently outperforms all other methods at a performance of 62.6% visible transmittance and an IR modulation of 34.7%, although the window does not allow clear imaging in its high-temperature form.[17] Nevertheless, progress has been hampered by the difficulty of synthesizing monodisperse, high-crystallinity nanoparticles using a low-temperature, ambient-atmosphere, simple technique. Two main synthetic methods have been studied, each with their own drawbacks. Hydrothermal synthesis can produce a nanoparticle powder although it requires a prolonged reaction time of 24 h or more under high pressures. Sol–gel, on the other hand, requires high temperatures of 400 °C or above, and the particles must be formed directly on the desired surface, hindering the use of a flexible low-temperature polymer substrate. Despite these synthetic and nanofabrication drawbacks, simulations suggest that the VO$_2$ composite path is the most

promising route to enhance the performance metrics and augment the potential for large scale use of VO$_2$ in thermochromic windows.[18]

In this paper, we present simulations that suggest taking advantage of the tunability of the plasmon resonance in metallic VO$_2$ could lead to the highest performing thermochromic windows to date. We demonstrate the feasibility of this approach by creating VO$_2$ nanoparticle composites in a flexible elastomer. A high-yield, low-temperature, ambient-pressure reaction was used to create high-quality VO$_2$ nanoparticles, which were then mixed with polydimethylsiloxane (PDMS) in a simple film fabrication method. We were able to achieve an 11.9% IR modulation at 50.7% clear visible transmittance using a fabrication method that is substrate independent and has tunable performance. The optical and elastomeric properties of the VO$_2$ colloidal films were thoroughly investigated, highlighting the beneficial effect of stretching the elastomeric matrix on the thermochromic performance of the composite.

2. Results and Discussion

2.1. Colloidal Film Simulations

Simulations exploring the optical properties of VO$_2$ nanoparticles have noted the importance of the surface plasmon of metallic VO$_2$ (R) with a resulting absorption peak around ≈1.2 µm.[19] The effect of the particle size and shape on the plasmon resonance has also been studied, noting the changes in spectral location and width of this resonance by tuning the size and the aspect ratio.[20] However, the ability to tune the plasmon resonance spectral position has not been fully utilized to enhance IR modulation.[21] In order to maximize performance, the plasmon resonance must be tuned to the IR spectral range with the highest solar irradiance, which is concentrated between 0.8 and 1.2 µm. To understand the relationship between nanoparticle size and plasmon resonance position, and to predict the potential performance of VO$_2$ elastomer colloidal films, Mie scattering simulations were employed. The diameter of VO$_2$ spherical nanoparticles was varied from 10 to 200 nm within a PDMS matrix. The resulting extinction efficiency, $Q_{ext}(\lambda)$, for

each particle was calculated as a function of wavelength, λ, and converted into a transmittance spectrum, %$T(\lambda)$, using

$$\%T(\lambda) = \exp(-Nl\pi r^2 Q_{ext}(\lambda)) \tag{1}$$

where N is the number of nanoparticles per unit volume, l is the film thickness, and r is the radius of the nanoparticle for calculating the geometrical cross section, πr^2.[22] N can be parameterized to depend on the weight percent, w, of nanoparticles as $N = N_{max} w$, where N_{max} is the maximum number of particles per unit volume assuming a close-packed simple cubic lattice of VO$_2$ nanoparticles. The visible transmittance figure of merit, T_{vis}, was calculated separately for VO$_2$ (M) and VO$_2$ (R) using:

$$T_{vis} = \frac{\int \%T(\lambda)\phi(\lambda)d\lambda}{\int \phi(\lambda)} \tag{2}$$

where $\phi(\lambda)$ is the AM1.5G solar irradiance and the integral runs from $\lambda = 350$ to 750 nm and then the two values were averaged. The IR modulation, ΔT, was calculated using Equation (2) with an integral from $\lambda = 750$ to 2000 nm for both VO$_2$ (M) and VO$_2$ (R) and taking the difference

$$\Delta T = T_{IR}^M - T_{IR}^R \tag{3}$$

The experimentally tunable parameters l and w in Equation (1) were varied such that their product, lw, ranged from 0.0005 to 0.15, and then T_{vis} and ΔT were calculated using Equations (2) and (3) to obtain the possible performance values at each particle diameter.

The Q_{ext} spectra in **Figure 1**A show a distinct peak at near-IR wavelengths that red shifts with increasing particle diameter from less than 1 µm to nearly 2 µm. The use of a dielectric matrix, as opposed to air, enhances the plasmon resonance by changing the permittivity, boosting overall performance.[20] The spectral position of the plasmon resonance with respect to the solar irradiance intensity dictates the performance values achievable. A 10 nm VO$_2$ nanoparticle colloidal film can achieve a performance of 50% IR modulation at a visible transmittance of 50% because of the placement of the plasmon resonance at ≈1 µm, where there is strong IR solar irradiance. On the other hand, a 200 nm particle cannot achieve any IR modulation at any visible transmittance because the plasmon resonance is tuned to ≈2 µm, where there
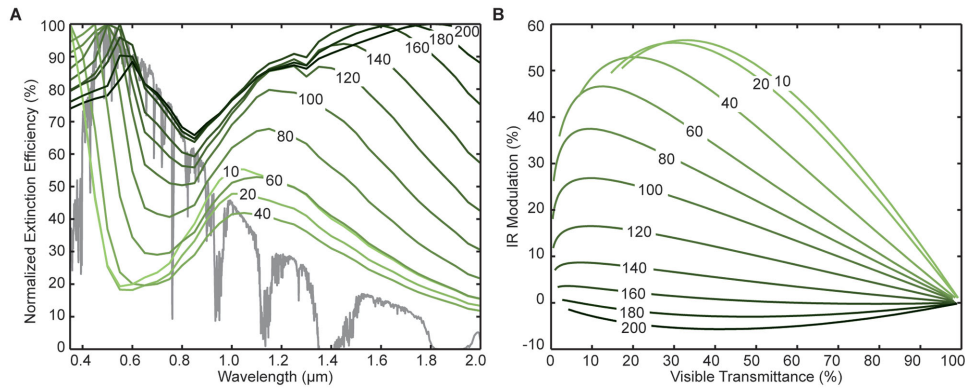

Figure 1. Optical simulation data of PDMS embedded with spherical VO$_2$ nanoparticles ranging in diameter from 10 to 200 nm. A) Normalized extinction efficiencies, Q_{ext} (green curves) for VO$_2$ in the metallic R phase with various nanoparticle diameters. Gray curve depicts the AM1.5G solar irradiance. B) Correlation of IR modulation, ΔT, with visible transmittance, T_{vis}, for each particle diameter. Curves at each diameter correspond to the product lw ranging from 0.15 on the far left to 0.0005 on the far right. All labels in panels (A) and (B) are in units of nanometers.
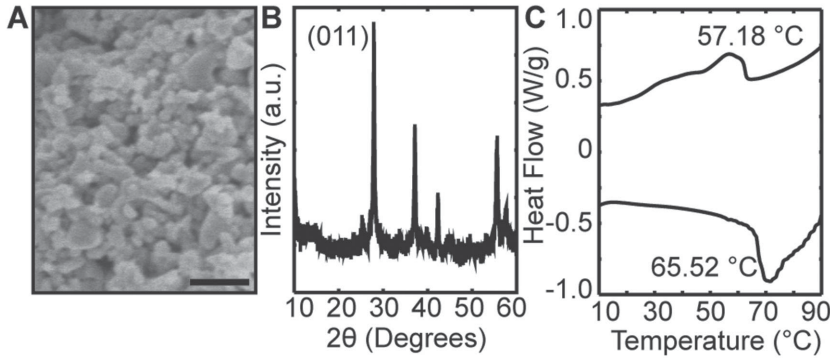
Figure 2. Characterization of VO₂ nanoparticles. A) SEM image of nanoparticles with an average size of 45 nm. Scale bar 200 nm. B) XRD pattern of as-synthesized nanoparticles. C) DSC of nanoparticles shows SMT temperatures of ≈66 °C and ≈57 °C.

is negligible solar irradiance. Intelligently using the nanoparticle size to tune the plasmon resonance within a transparent dielectric matrix could enhance the performance of VO₂ windows to achieve significantly higher performances than those reported to date.

2.2. Nanoparticle Synthesis

The simplicity of a colloidal film design coupled with potentially impressive performance, as suggested by the simulations, is the impetus to experimentally pursue VO₂ colloidal films. There are a few requirements for the synthesis and film fabrication if it is to be a simple and economically viable option for widespread adoption of thermochromic windows. First, all procedures must be carried out at low temperature and in ambient atmosphere to ensure industrial scalability of resulting films. Second, the synthesis must produce nanoparticles in solution that can be dried to a powder in order to be incorporated into a polymer solution and deposited on arbitrary substrates. Here, a slight modification of a facile, low-temperature, ambient-condition synthesis was used to achieve a high yield of VO₂ nanoparticles.[23] This synthesis relies on the conversion of vanadyl ethylene glycolate (VEG) to VO₂ through thermolysis, which affords a high yield of nanoparticles with an average diameter of 42 ± 39 nm (**Figure 2**A). By synthesizing VO₂ through thermolysis, the preferential rod crystal growth is bypassed.[24] Based on our simulations, the spherical shape and sub-100 nm size selection provided by this synthesis is essential for the performance of the VO₂ films. X-ray diffraction (XRD) spectra (Figure 2B) confirm full conversion of VEG to VO₂ by the strong peak at 27.8° (JCPDS card no. 44-0252). The direct conversion to VO₂ (M) ensures that there are no other VO₂ crystal phases present. Finally, differential scanning calorimetry (DSC) in Figure 2C shows that the SMT occurs at a temperature of ≈66 °C upon heating and ≈57 °C upon cooling, with a hysteresis of 9 °C. The transition temperature and wide hysteresis are typical of VO₂ nanoparticles.[25]

2.3. Film Fabrication and Optical Analysis

Our simulations show that varying *lw* should result in a range of performances, so films with varying film thickness and a

constant nanoparticle concentration were fabricated by suspending the as-synthesized nanoparticles in a dilute PDMS solution and dropcast on glass substrates. This simple fabrication method created high-quality films with thicknesses ranging from ≈15 to ≈75 μm.

Figure 3A,C,E shows the visible film quality with varying thicknesses, with examples of the thinnest, thickest, and intermediate films. There is a slight brownish tint to the films, and the relatively minimal scattering makes the background design clearly visible through the films. Figure 3B,D,F shows dark-field microscopy images, in which the increase in background color with film thickness shows the increase in the number of small nanoparticles, and the minimal amount of bright dots suggests a small number of particle aggregates or large nanoparticles. The uniform dispersion of nanoparticles within the film is essential for obtaining high performance because it minimizes large scattering centers that do not exhibit the desired plasmon resonance (cf. Figure 1). Finally, the optical properties of each film were studied at room temperature and above the SMT temperature, at 80 °C, as shown in Figure 3G,H,I. The high transmittance at long wavelengths shows the high quality of the films, as there should be negligible scattering or absorptance. The high absorptance at short wavelengths, giving the films their color, is expected due to the inter- and intraband absorptions of VO₂.[6] At high temperature, the metallic VO₂ nanoparticle plasmon resonance absorbs most predominantly around 1.2 μm, which causes the decrease in IR transmittance at the same spectral position.[19] This observation is qualitatively in agreement with simulations; however, simulations predict that the absorptance peak at the plasmon resonance should be more intense and narrower than the broad peak observed experimentally. This discrepancy can be reasonably explained by the large size distribution of synthesized nanoparticles within the film, effectively averaging over a distribution of plasmon resonances, as well as the 5% of nanoparticle diameters above 100 nm. A small number of rod-shaped particles within the sample may also contribute to broadening of the plasmon resonance.[26] The visible transmittance decreases with an increase in film thickness, offset by an equal increase in absorptance, as expected.[27] The reflectance is consistently low for each film thickness across all wavelengths.

The performance of VO₂ films as a function of film thickness, with constant VO₂ nanoparticle concentration, is summarized in **Figure 4**. The IR modulation for absorptance and transmittance nearly overlap, showing that the performance is solely due to the increase in absorptance, which ultimately relies on the metallic VO₂ plasmon resonance. This result is in contrast to what is seen in VO₂ thin films, where the change in reflectance and absorptance both contributes to the IR modulation.[19] The performance was tuned from an IR modulation of 0.97% at a visible transmittance of 85.8% to an IR modulation of 11.9% at a visible transmittance of 50.7%. It is expected that increasing the nanoparticle concentration rather than increasing the film thickness would produce a similar trend.
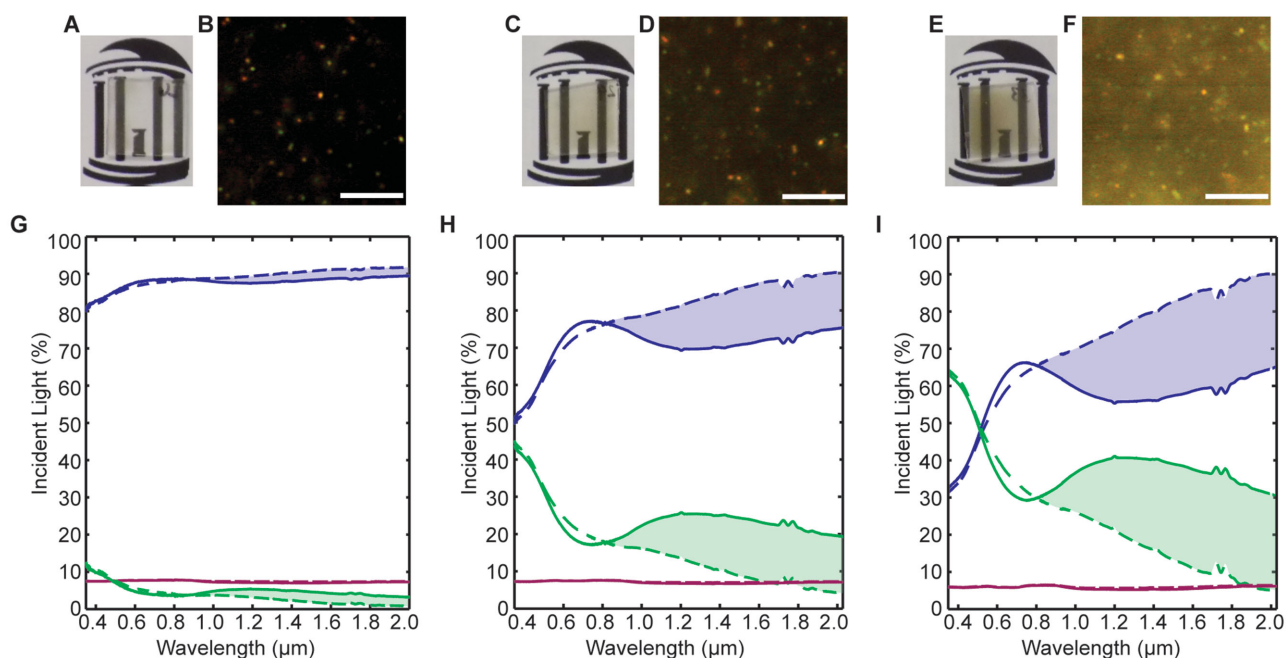
Figure 3. Optical properties of representative films where the left column A,B,G) is an ≈15 μm thick film, the middle column C,D,H) is an ≈40 μm thick film, and the right column E,F,I) is an ≈75 μm thick film. A,C,E) Macroscale images of respective films. B,D,F) Dark-field images of respective films, showing an increase in particle concentration via color change as well as high dispersity of nanoparticles. Scale bar 8 μm. G,H,I) Optical properties of individual VO$_2$ films, where blue is transmittance, green is absorptance, and pink is reflectance. The dashed line indicates room-temperature optical measurements for each color, and the thick line indicates high-temperature optical measurements.

2.4. Elastomer Properties Result

We also examined the elastomeric properties of the colloidal films and their influence on the optical properties and thermochromic performance. The elastomer matrix allows the thickness of the films to be modulated simply by stretching. The stability and mechanical properties seem consistent with that of pure PDMS. The film was peeled from the glass substrate on which it was prepared, stretched, and measured for visible and IR transmittance as before. For the film shown in

Figure 5, the performance values achieved were 45.6% visible transmittance and an IR modulation of 7.6%. The film was then stretched ≈36% and the transmittance was measured again, producing a visible transmittance of 55.4% and an IR modulation of 8.1%. The general shape of the transmittance spectra of both the stretched and unstretched films are similar to the films on the glass substrate, and the broad resonance is still clearly present.

Remarkably, the overall performance for both visible and IR figures of merit improved upon stretching the film. The T_M-T_R spectrum (Figure 5B) was calculated by taking the difference between the high-temperature transmittance curve and the low-temperature transmittance curve, and it shows a slight blueshift of the stretched film. This effect can be explained by a change in the morphology of the film upon stretching (Figure 5C). As the film is stretched, the film thickness decreases, but the volume concentration of nanoparticles stays constant because the Poisson ratio of PDMS is 0.5 and the film is effectively incompressible. Stretching the film induces strain onto the composite film, which is localized into high-stress regions centered around the nanoparticles. Voids are then likely to form at these high-stress areas due to the ease of delamination at the interface of PDMS (hydrophobic) and the VO$_2$ nanoparticles (hydrophilic). Similar effects have been observed in other elastomer
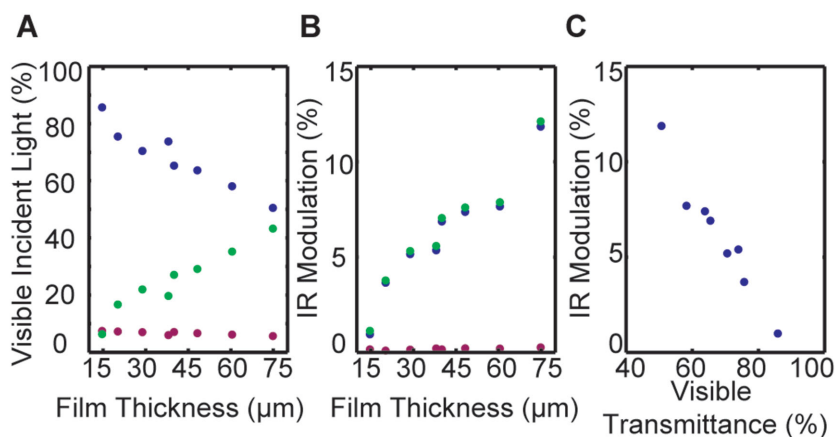

Figure 4. Performance values for films varying in thickness from ≈15 to ≈75 μm. A) Percentage of visible light transmitted (blue), absorbed (green), and reflected (pink). B) Percentage of IR light modulated by transmittance (blue), absorptance (green), and reflectance (pink) for the same films. C) Range of performances achievable by modulating the thickness of the film.
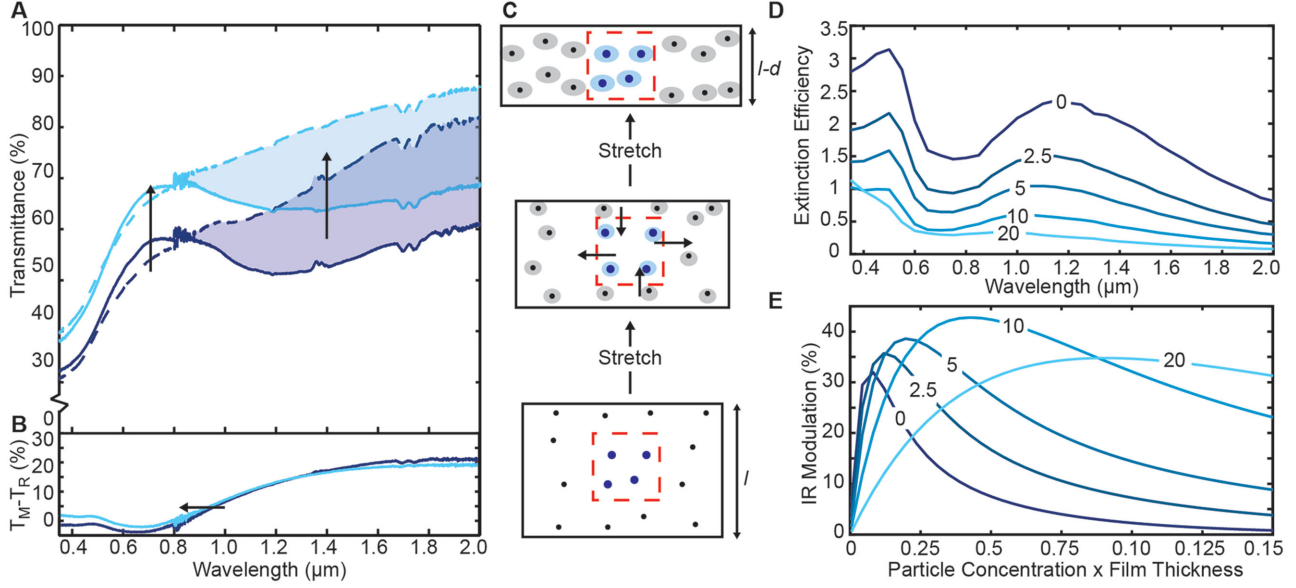
Figure 5. Effect of elastomeric properties of the film on thermochromic performance. A) Transmittance spectrum of the unstretched film (dark blue) and the stretched film (light blue), where the dashed line indicates room-temperature transmittance and full line indicates high-temperature transmittance. B) T_M-T_R spectrum of the stretched (dark-blue curve) and unstretched (light-blue curve), showing the slight blueshift of the stretched film. C) Schematic of the change in film morphology and volumetric concentration upon stretching. D) Extinction efficiency, Q_{ext}, of a 90 nm VO$_2$ nanoparticle with varying shell thicknesses of air from 0 to 20 nm, all embedded in a PDMS matrix. E) Resulting IR modulation values at varying lw values ranging from 0.0005 to 0.15.

composites.[28] The decrease in thickness, Δl, is the primary reason for the increase of visible transmittance upon stretching the composite film, as can be seen through the modification of Equation (1) to

$$T_{vis}^{Stretch} = T_{vis} + \Delta l N \pi r^2 Q_{ext} \tag{4}$$

where Δl is small. However, this equation does not fully explain the improvement in IR modulation. Mie scattering simulations (Figure 5D) show that the introduction of a shell of air, which represents the presence of a void in the near-field of the particle, positively contributes to both the visible transmittance and IR modulation. The air shell decreases the extinction efficiency because of the introduction of a lower refractive index material. This decrease in extinction efficiency increases the visible transmittance of the films overall. The plasmon resonance spectral position is also affected, shifting from ≈1.2 to ≈1 µm with the introduction of an air shell. This shift is beneficial to the IR modulation as the plasmon resonance spectral position of VO$_2$ in air is closer to region of higher solar irradiance. The experimentally observed blueshift of the stretched T_M-T_R spectrum does support the overall shift of plasmon resonances expected upon stretching.

The potential IR modulation was then calculated at lw values of 0.0005–0.15, and it can be seen (Figure 5E) that the IR modulation does increase by introducing a shell of air up to a shell thickness of 20 nm, caused by the improved position of the plasmon resonance relative to the solar spectrum. At a sufficiently large air shell thickness, such as 20 nm, the effective refractive index of the scattering center reduces the advantageous scattering effect. The introduction of a small air shell at a constant w while decreasing l should give a large increase in IR modulation. Experimentally, the increase in IR modulation we

observe is consistent with this analysis but is somewhat smaller than expected, probably again due to the large distribution of nanoparticle sizes and therefore the air shell thicknesses. The ability to improve visible transmittance and simultaneously improve IR modulation simply through stretching the elastomeric colloidal film is a unique way to increase performance. This improvement introduced by air pockets, as explored through simulation, opens the door to a new potential avenue for improving thermochromic film performance.

3. Conclusion

Simulations demonstrated that VO$_2$ PDMS colloidal films had the potential of outperforming all current thermochromic windows, and we have shown that this approach is experimentally viable. We have fabricated VO$_2$ elastomer colloidal films using a low-temperature, scalable synthesis, and an overall simple fabrication method. By tuning film thicknesses, performance ranged from 0.97% IR modulation at 85.8% visible transmittance to 11.9% IR modulation at 50.7% visible transmittance. Optical extinction analysis elucidated the importance of plasmon resonance in the IR modulation and thus in the performance of the thermochromic window. Upon stretching, the performance increases from 45.6% visible transmittance and an IR modulation of 7.6% to 55.4% visible transmittance and an IR modulation of 8.1%. We have experimentally demonstrated the viability of these films for real applications, and we have shown through simulations that by tuning the nanoparticle size and thus the plasmon resonance, it is possible to achieve 50% IR modulation and 50% visible transmittance within this framework. The impact of the plasmon resonance on performance is clear, and it

can be shifted to a more optimal spectral position by stretching the elastomer colloidal films. In order to improve performance overall, the synthesis must be improved by both decreasing the nanoparticle size and the size distribution. Additionally, the developed approach can be used in tandem with other known methods for improving overall performance, such as doping the nanoparticles to lower SMT temperature or placing it in temperature-sensitive performing polymers.

4. Experimental Section

Simulations: Extinction efficiency values for spherical VO_2 (M) and VO_2 (R) nanoparticles ranging in diameter from 10 to 200 nm in a PDMS matrix (refractive index = 1.4) were obtained using the Mie Theory Calculator program with previously reported optical data.[29,30] Introduction of air pockets was simulated by a 2.5–20 nm thick shell of air around a VO_2 90 nm particle, all embedded in a PDMS matrix. The resulting extinction efficiency values were used to calculate transmittance spectra for VO_2 (M) and VO_2 (R) at 40 *lw* values ranging from 0.0005 to 0.15. These transmittance curves were used to calculate visible transmittance and IR modulation figures of merit at each *lw* value, for each particle size.

Nanoparticle Synthesis: Nanoparticle synthesis was adopted and modified slightly. Briefly, ammonium metavanadate (0.5 g, Fisher Scientific) was added to ethylene glycol (10 mL, Fisher Scientific) at 160 °C and heated with vigorous stirring for 2 h. The dark VEG precipitate was collected by vacuum filtration and washed with ethylene glycol. Two drying steps of 30 min at 250 °C in a Petri dish followed with additional wash and rinse in between. The resulting dark blue VO_2 (M) powder was collected.

Film Fabrication: The as-synthesized VO_2 nanoparticles (0.012 g) were added to a solution of PDMS (0.79 wt%, Sylgard 184, Dow Corning) in heptane with curing agent (7.7 wt%). The solution was sonicated for 1 h and then left to settle for 4 d until the solution changed from a dark blue/gray opaque solution to an orange/brown transparent solution. 50–200 µl (in 25 µl steps) of resulting solution was dropcast onto 1.5 cm x 1.5 cm glass slides. After 12 h of drying, the films were transferred dried in an oven at 150 °C for an additional 12 h. Upon removal, the films were entirely dry and cured. To make pure PDMS films, the PDMS was peeled off the glass substrate using a razor blade.

Analysis: VO_2 particle morphology, identity, and quality were measured with a Hitachi S-4700 Cold Cathode Field Emission Scanning Electron, a Rigaku Multiflex X-Ray Diffractometer with Cu source, and a TA Instrument DSC Q200, respectively. XRD spectra were taken from 10°–60° 2θ at a scan rate of 2° 2θ min^{-1}, where the powder was spread on a no-background sample holder. The DSC data were taken using a ramp of 5 °C min^{-1} and cooled at 10 °C min^{-1} from 0 to 100 °C in a Tzero hermetic aluminum pan. Film thickness was measured using a Bruker DektakXT profilometer, where the heights from five different line scans evenly spaced across the film were averaged together using the Vision 64 program. Optical pictures were taken using a Nikon D-Eclipse C1 si dark-field microscope (100× zoom) and macroscale pictures were taken using a Nikon DSLR camera. Optical properties of each film were measured in a Cary 5000 UV–vis–NIR from Agilent with integrating sphere attachment. Data were normalized against a glass standard to reduce effect of background spectra on the curvature of experimental data. High-temperature data were collected using a homebuilt heating stage with a TE Tech peltier stage that was attached to the UV–vis–NIR. Data were taken at room temperature (25 °C) and above the SMT temperature, 75–80 °C.

[1] Estimated U.S. Energy Use in 2014, https://flowcharts.llnl.gov/content/assets/images/energy/us/Energy_US_2014.png (accessed: August, 2015).
[2] International Energy Outlook 2013, http://www.eia.gov/todayinenergy/detail.cfm?id = 12251 (accessed: August, 2015).
[3] F. J. Morin, *Phys. Rev. Lett.* **1959**, *3*, 34.
[4] J. Nag, R. F. Haglund Jr., *J. Phys. Condens. Matter* **2008**, *20*, 264016.
[5] M. E. A. Warwick, R. Binions, *J. Mater. Chem. A* **2014**, *2*, 3275.
[6] Z. Chen, Y. Gao, L. Kang, J. Du, Z. Zhang, H. Luo, H. Miao, G. Tan, *Sol. Energy Mater. Sol. Cells* **2011**, *95*, 2677.
[7] N. R. Mlyuka, G. A. Niklasson, C. G. Granqvist, *Sol. Energy Mater. Sol. Cells* **2009**, *93*, 1685.
[8] N. R. Mlyuka, G. A. Niklasson, C. G. Granqvist, *Appl. Phys. Lett.* **2009**, *95*, 171909.
[9] X. Qian, N. Wang, Y. Li, J. Zhang, Z. Xu, Y. Long, *Langmuir* **2014**, *30*, 10766.
[10] X. Cao, N. Wang, J. Y. Law, S. C. J. Loo, S. Magdassi, Y. Long, *Langmuir* **2014**, *30*, 1710.
[11] Y. Gao, H. Luo, Z. Zhang, L. Kang, Z. Chen, J. Du, M. Kanehira, C. Cao, *Nano Energy* **2012**, *1*, 221.
[12] I. G. Madida, A. Simo, B. Sone, A. Maity, J. B. Kana Kana, A. Gibaud, G. Merad, F. T. Thema, M. Maaza, *Sol. Energy* **2014**, *107*, 758.
[13] S. Chen, L. Dai, J. Liu, Y. Gao, X. Liu, Z. Chen, J. Zhou, C. Cao, P. Han, H. Luo, M. Kanahira, *Phys. Chem. Chem. Phys.* **2013**, *15*, 17537.
[14] Y. Gao, S. Wang, L. Kang, Z. Chen, J. Du, X. Liu, H. Luo, M. Kanehira, *Energy Environ. Sci.* **2012**, *5*, 8234.
[15] Y. Li, S. Ji, Y. Gao, H. Luo, M. Kanehira, *Sci. Rep.* **2013**, *3*, 1370.
[16] C. Liu, X. Cao, A. Kamyshny, J. Y. Law, S. Magdassi, Y. Long, *J. Colloid Interface Sci.* **2014**, *427*, 49.
[17] Y. Zhou, Y. Cai, X. Hu, Y. Long, *J. Mater. Chem. A* **2015**, *3*, 1121.
[18] S.-Y. Li, G. A. Niklasson, C. G. Granqvist, *J. Appl. Phys.* **2010**, *108*, 063525.
[19] G. A. Niklasson, S.-Y. Li, C. G. Granqvist, *J. Phys. Conf. Ser.* **2014**, *559*, 012001.
[20] K. Laaksonen, S.-Y. Li, S. R. Puisto, N. K. J. Rostedt, T. Ala-Nissila, C. G. Granqvist, R. M. Nieminen, G. A. Niklasson, *Sol. Energy Mater. Sol. Cells* **2014**, *130*, 132.
[21] Y. Zhou, A. Huang, Y. Li, S. Ji, Y. Gao, P. Jin, *Nanoscale* **2013**, *5*, 9208.
[22] H. C. van de Hulst, *Light Scattering by Small Particles*, Dover Publications, New York **1981**.
[23] J. Zou, Y. Peng, H. Lin, *J. Mater. Chem. A* **2013**, *1*, 4250.
[24] Y. Gao, C. Cao, L. Dai, H. Luo, M. Kanehira, Y. Ding, Z. L. Wang, *Energy Environ. Sci.* **2012**, *5*, 8708.
[25] R. Lopez, T. E. Haynes, L. Boatner, L. C. Feldman, R. F. Haglund, *Phys. Rev. B* **2002**, *65*, 224113.
[26] R. Lopez, T. E. Haynes, L. A. Boatner, L. C. Feldman, R. F. Haglund, *Opt. Lett.* **2002**, *27*, 1327.
[27] G. Xu, P. Jin, M. Tazawa, K. Yoshimura, *Jpn. J. Appl. Phys.* **2004**, *43*, 186.
[28] D. Ge, E. Lee, L. Yang, Y. Cho, M. Li, D. S. Gianola, S. Yang, *Adv. Mater.* **2015**, *27*, 2489.
[29] H. W. Verleur, J. A. S. Barker, C. N. Berglund, *Phys. Rev.* **1968**, *172*, 788.
[30] I. Charamsinau, The Mie Theory Calculator, http://lyle.smu.edu/ee/smuphotonics/MieTheoryCalculator/MieTheoryCalculator.htm (accessed: March, 2015).